University of Groningen

Microscopy imaging and modeling study on the mechanical properties of the primary flight feather shaft of the bean goose, Anser fabalis

Liu, Chao; Xu, Lihan; Li, Xiujuan; Liu, Yansong; Qi, Yingchun; Sun, Jiyu; Zou, Meng

IMPORTANT NOTE: You are advised to consult the publisher's version (publisher's PDF) if you wish to cite from it. Please check the document version below.

Document Version
Publisher's PDF, also known as Version of record

Publication date:
2022

[Link to publication in University of Groningen/UMCG research database](#)

RESEARCH ARTICLE

Microscopy imaging and modeling study on the mechanical properties of the primary flight feather shaft of the bean goose, *Anser fabalis*

Chao Liu[1,2] 🄳 | Lihan Xu[1] | Xiujuan Li[1] 🄳 | Yansong Liu[1] 🄳 | Yingchun Qi[1] 🄳 |
Jiyu Sun[1] 🄳 | Meng Zou[1] 🄳

[1]Key Laboratory of Bionic Engineering (Ministry of Education, China), Jilin University, Changchun, China

[2]Faculty of Science and Engineering, University of Groningen, Groningen, The Netherlands

Correspondence
Meng Zou, Key Laboratory of Bionic Engineering (Ministry of Education, China), Jilin University, Changchun, 130022, China.
Email: zoumeng@jlu.edu.cn

Abstract
Avian flight feathers have the unique advantages of lightweight and high strength, which play a key role in their flight capacity. In this article, the rachis of the bean goose's primary flight feather was used as the research object. Its compressive properties were analyzed and the 3D microscale was observed by 3D microscope system with a super wide depth of field. The distribution of mechanical properties, section variation of fiber and internal microstructure of rachis were obtained by micro-CT technique. Based on these results, a 3D reconstructed model was established for structure mechanical simulation. The simulation results were close basically to the compressive strength of the actual sample. These results show that the synergistic effect of cortex and medulla can improve mechanical resistance of the rachis. Therefore, the best position (N3) of the primary flight feather shaft can be applied to the bionic design of thin wall structures for energy absorption. This research can provide some guidance for the application of lightweight structural design.

Research Highlights
1. The internal structure of bean goose feather shaft was observed by micro-CT.
2. The experimental method has a deeper understanding of the compressive properties of rachis fiber orientation.
3. Under the synergistic effect of cortex and medulla, the compressive performance of rachis is better.

KEYWORDS
bean goose's primary flight feather, fiber orientation, mechanical properties

1 | INTRODUCTION

Avian feathers (including the vane and the shaft) have many excellent characteristics (Sullivan et al., 2017), the most obvious being the mechanical properties of lightweight and high strength. Flight feathers are unique among all kinds of keratin appendages. The rachis is a complex thin-walled structure that meets all the design standards of lightweight and high-strength, and has excellent

mechanical adaptability. In recent years, more and more researches about the biological characteristics of feathers have been applied to the engineering field (Sullivan et al., 2019). There are many studies on the vane, such as the recovery performance and microstructure of bird feathers (Zhao et al., 2020), the connection pattern (Chen et al., 2020) and the arrangement mode of barbule (McCoy et al., 2018), and so forth. The results better explain the reasons for birds flying. It provides a reference for the design of new bionic

interlocking materials. However, the rachis also plays an important role that cannot be ignored.

The rachis of birds is light, hard, and strong, and its cortex is composed of various fiber layers (Laurent et al., 2019). It is an important connecting body of the feathers (Xing et al., 2019). The airflow penetration structure along the shaft can significantly reduce resistance (Eder & Fiedler, 2017). The feather shaft is composed of calamus and rachis (Schelestow et al., 2017). The former is a hollow tubular structure, which is the foundation of the shaft, and the latter is longer and supports the upper vane. Some researchers have found that the inner part of the rachis is entirely composed of β-keratin, which is the hardest known natural polymer (Astbury & Marwick, 1932; Wang et al., 2016). Ventral curvature of the rachis can increase the proximal lateral force (Oorschot et al., 2020). Studying the failure mechanism of feather calamus and rachis after compression, it is found that the foam medulla has a great influence on the mechanical response of the specimen and the energy dissipated in the test (Schelestow et al., 2017). Raman spectroscopy was used to study the difference in the protein secondary structure between the inner and outer areas of the rachis cortex, and the inner area is harder than the outer area to avoid further buckling (Laurent et al., 2020). At the same time, it is found that the rachis will swell and soften after the bending failure after the hydration step, which will make the harder buckling fibers reposition to the initial position, and the strength will be restored after drying (Sullivan et al., 2018). Mechanical properties of the rachis of different parts of birds are very different. The mechanical properties of the rachis of the primary flight feathers are better than those of the secondary flight feathers, tail feathers and alula feathers (Zou et al., 2019; Zou et al., 2020). Wang studied the layered fiber and porous structure of the primary flight feathers along the rachis length (Wang & Meyers, 2016). However, there are few studies on the continuous mechanical properties of rachis fiber orientation. The mechanical properties of different areas of rachis fiber orientation are also very different. Finding the optimal area can pave the way for the design of thin-walled structures.

In this article, the cross-sectional microstructure, mechanical properties, and energy absorption mechanism of the rachis of bean goose's primary flight feathers in different regions were studied. The compression simulation test of the 3D reconstruction model was carried out by Ansys Workbench software, and discovered the structural parts that determine the good mechanical properties of the rachis. This research provides relevant enlightenment and reference for the design of anti-compression bionic structure.

2 | MATERIALS AND METHODS

2.1 | Compression test

The primary flight feathers of bean goose (*Anser fabalis*) used in this experiment were collected from Jilin Province Qian Xiyin Animal Specimen Co., Ltd. The feather samples (Figure 1) were cut off from the wings of the newly dead bean goose with scissors attached to the roots of the primary flight feather. And the feather roots were
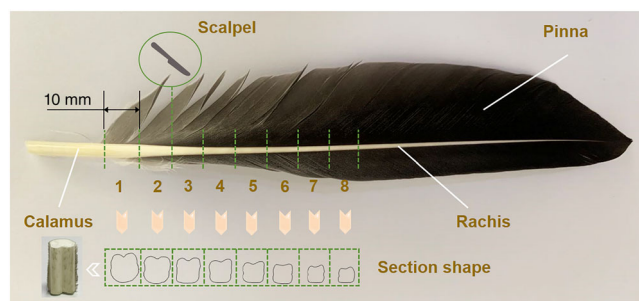
FIGURE 1 The primary flight feather of bean goose and the diagram of different section position

wrapped immediately with plastic wrap for avoiding water evaporation. The compressive performance test samples were divided into three groups, each group has three samples, which were used for the axial compression test, the axial compression test after removing the medulla, and the three-point bending test, respectively.

From thicker side of the rachis, these samples were cut out eight parts in sequence along the fiber direction interval 10 mm, as shown in Figure 1. The both sides of the rachis sample were polished by No.2000 sandpaper to ensure flat. A small electronic universal testing machine (AG-X, SHIMADZU, Japan) with a measuring range of 1 kN was used to study the mechanical properties of the bean goose's primary flight feather rachis in the fiber direction. The length of the sample did not more than 3.5–4 times the thickness, which can keep vertical between sample and loading platform. The eight samples were numbered N1–N8, respectively. In order to study the effect of the rachis' medulla under the same conditions, a comparative test was designed with rachis without medulla. Therefore, the sample's medulla was removed by stainless steel high-precision pointed tweezers until the residual did not more than 5%. The eight samples were numbered S1–S8, respectively. The measured sample parameters including the width, thickness, length and mass are shown in Table 1. The prepared samples were placed the indenter of the testing machine, the loading speed was set to 2 mm/min and the sampling rate was set to 10 Hz.

2.2 | Three-point bending test

Similarly, from thicker side of the rachis, the length of the sample was calculated based on the thickness along the fiber direction. The three samples (F1–F3) were cut in sequence with a sharp blade, as shown in Figure 2a. The width, thickness, length, and mass of each sample were measured, and the span was calculated. The sample parameters are shown in Table 2. The dorsal side of the rachis was placed under the indenter, the loading speed was set to 0.8 mm/min until the specimen is crushed.

2.3 | Structural analysis test

Before the compression test, the cross-sections of eight rachis specimens were observed by the 3D microscope system with a super wide

TABLE 1 The sample parameters of compression test of the primary flight feather shaft

| Specimen | | The size of rachis | | | |
| | | Width | Thickness | Length | Mass |
		D1/mm	D2/mm	L/mm	M/mg
With medulla	N1	4.6 ± 0.5	4.1 ± 0.3	10.2 ± 0.9	40.9 ± 2.8
	N2	4.0 ± 0.3	3.8 ± 0.5	10.6 ± 1.7	38.3 ± 5.1
	N3	3.5 ± 0.5	3.6 ± 0.2	10.3 ± 1.1	33.4 ± 3.2
	N4	3.4 ± 0.1	3.2 ± 0.5	9.8 ± 1.3	29.0 ± 4.6
	N5	3.1 ± 0.1	3.0 ± 0.4	9.9 ± 1.6	26.8 ± 3.7
	N6	2.9 ± 0.2	2.7 ± 0.4	9.4 ± 0.3	23.3 ± 2.2
	N7	2.7 ± 0.2	2.5 ± 0.5	9.4 ± 0.3	20.6 ± 3.4
	N8	2.5 ± 0.2	2.3 ± 0.5	8.8 ± 0.5	17.3 ± 3.7
Without medulla	S1	5.1 ± 0.0	4.5 ± 0.1	10.3 ± 1.0	41.6 ± 5.6
	S2	4.5 ± 0.1	4.2 ± 0.1	11.0 ± 0.6	40.1 ± 2.3
	S3	4.1 ± 0.0	3.9 ± 0.1	10.1 ± 0.2	33.3 ± 1.3
	S4	3.7 ± 0.1	3.6 ± 0.1	9.8 ± 1.0	30.6 ± 4.4
	S5	3.5 ± 0.1	3.4 ± 0.0	10.7 ± 0.2	31.8 ± 0.1
	S6	3.3 ± 0.0	3.2 ± 0.0	10.0 ± 0.4	26.9 ± 1.4
	S7	3.1 ± 0.0	3.0 ± 0.0	10.2 ± 0.8	25.5 ± 1.9
	S8	3.0 ± 0.0	2.9 ± 0.1	10.5 ± 0.1	25.7 ± 0.3

FIGURE 2 The three-point bending test diagram (a) the preparation of the rachis specimen; (b) the test process under quasi-static load from the initial state to termination state

depth of field (VHX-5000, KEYENCE, Japan), obtaining the change rule of the rachis section in the fiber direction, as shown in Figure 1. Micro-CT (Xradia 610, Zeiss, Germany) was used to obtain the internal structure of the best mechanical properties sample, the detail was shown in Figure 3. The internal microstructure of the sample can be observed through high-contrast scanning imaging. The scan parameters are shown in Table 3.

The scan result provided the accurate quantitative and qualitative information about the 3D shape of the sample (Saey & Dietmar, 2006). The 2009 slice images of different positions with a resolution of 2269 × 2108 were exported. Then, the 3D model was built by importing these slices into Solidworks 2016, and its mechanical properties were analyzed by Ansys Workbench 19.2.

2.4 | The evaluation index of mechanical performance

(1) Specific energy absorption: It is the energy absorbed by the unit mass of the structure, and it represents the utilization rate of the material in the energy absorption of the structure during the collision. Its calculation formula is shown as Equation (1):

$$SEA = \frac{E_{total}}{M} = \frac{\int Fds}{M}. \tag{1}$$

(2) Mean crush force: It represents the ratio of the energy absorbed by the plastic deformation of the thin-walled tube to the deformation displacement of the thin-walled tube during the collision. Its calculation formula is as Equation (2):

$$F_{MCF} = \frac{E_{total}}{d} = \frac{\int_0^d f(x)dx}{d}. \tag{2}$$

TABLE 2 The sample parameters of three-point bending test of primary flight feather shaft

| | The size of rachis | | | | |
| | Width | Thickness | Length | Mass | Span |
Specimen	D1/mm	D2/mm	l/mm	M/mg	L/mm
F1	3.92 ± 0.23	3.70 ± 0.21	53.65 ± 3.18	198.73 ± 23.94	44.50 ± 2.38
F2	2.72 ± 0.18	2.64 ± 0.17	38.64 ± 1.81	92.88 ± 11.04	32.00 ± 1.73
F3	2.07 ± 0.17	2.10 ± 0.15	29.78 ± 2.38	46.20 ± 7.87	25.25 ± 1.71
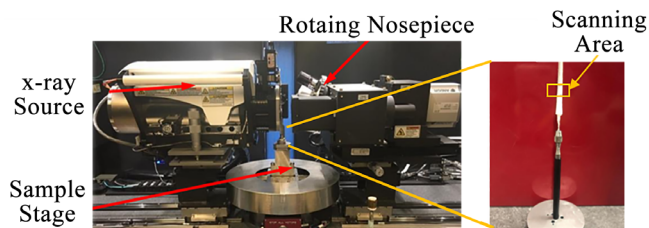
FIGURE 3 Micro-CT (Xradia 610) versa 3D X-ray microscope. The internal structure of sample can be obtained

(3) Compressive strength: It refers to the strength limit when an external force exerts pressure. Its calculation formula is as Equation (3):

$$\sigma = \frac{F}{S}. \tag{3}$$

(4) Young's modulus: It is the physical quantity of the tensile or compressive resistance of a material within the elastic limit. Its size indicates the rigidity of the material. The greater the Young's modulus, the less likely to be deformed. Its calculation formula is shown as Equation (4):

$$E = \frac{\sigma}{\varepsilon} = \frac{F/S}{dL/L}, \tag{4}$$

where, σ represents linear stress, ε represents linear strain.

(5) Bending strength refers to the ability of a material to resist bending without breaking, and its standard formula is as follows:

$$\sigma_f = \frac{3FL}{2bh^2}, \tag{5}$$

where, F is the instantaneous load, L is the span, b is the width of the sample, and h is the thickness of the sample.

3 | RESULTS AND DISCUSSION

3.1 | Compression test

3.1.1 | Compression test of rachis with medulla

Compression tests were carried out on longitudinal different areas of the primary flight feather shaft, and the maximum elastic modulus of each sample before reaching the maximum stress was taken, as shown in Figure 4a. It can be seen that the elastic modulus of the rachis increases gradually along the fiber direction.

It can be seen from Figure 4b that the mean crushing force from the root of the rachis first increases and then decreases in the fiber direction, while the specific energy absorption first increases and then decreases and gradually stabilizes. In Figure 4c, the compressive strength first increases and then basically stabilizes. Higher specific energy absorption and average load means better energy absorption, and higher compressive strength means better compressive resistance. Comprehensive analysis shows that the mechanical properties of the N3 sample are the best.

3.1.2 | Compression test of rachis without medulla

As shown in Figure 5a, comparing the rachis specimens with medulla, it is found that the specific absorption energy of rachis without medulla is significantly reduced, which is basically consistent with the change law of rachis with medulla. Moreover, it can be seen from Figure 5b that the loaded region of N1 rachis with medulla is large after compression, after reaching the peak, it slowly weakens and then increases again. First, one end of the specimen begins to deform, and then after the pressure reaches a certain value, the stress increases again, and the medulla is again involved in cooperating with the cortex to resist the pressure.

From Figure 5c, there were no medulla. The S1 sample fractured rapidly after compression to the maximum stress, indicating that the rachis without medulla became more brittle, easier to fracture, and the loaded region was also reduced. The comparison found that the cortex and medulla synergistic effect on the rachis compression performance is better. At the same time, it shows that the medulla is light in weight, but it has a great influence on the energy absorption and mechanical properties of the shaft.

3.2 | Three-point bending test

From Figure 2b, the sample was placed on the two supports. When the sample breaks or its displacement dropped to 5 mm, the test was stopped. Figure 6a shows that the total energy absorption of the three continuous segments in fiber direction of the rachis showed a significant decrease, and the specific energy absorption gradually increased, but its increase range was small. Taking into account, the

|	Voxel (μm)	Vision scope (mm)	Energy/power (kV/W)	Scanning time (hours)
Rachis	2.25	Φ4.5	40/3	2.0

TABLE 3 The micro-CT scan parameters of the sample
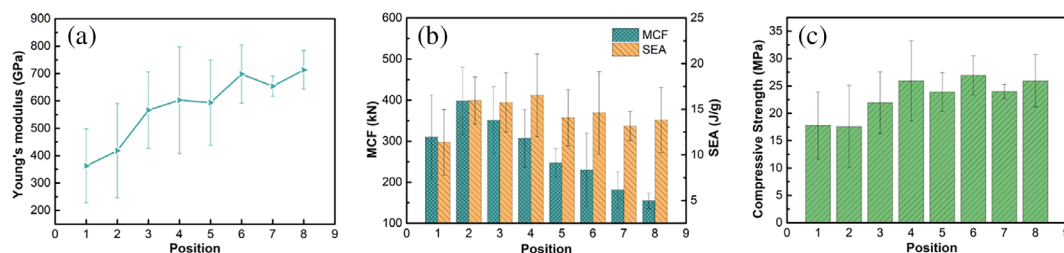
FIGURE 4 The distribution law of the mechanical properties of the primary flight feather shaft fiber orientation in different areas: (a) elastic modulus, (b) mean crushing force and specific energy absorption, (c) compressive strength
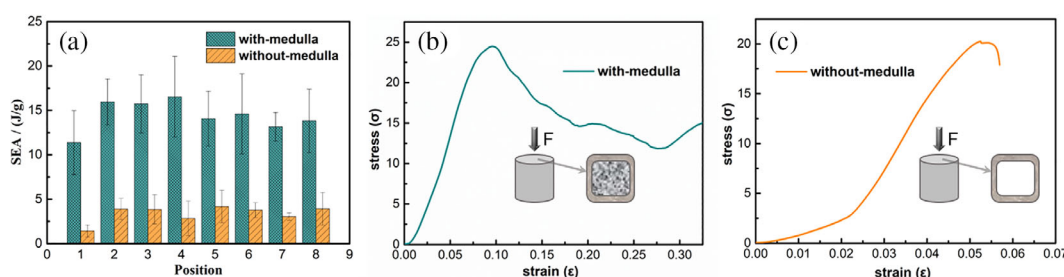
FIGURE 5 The influence of the medulla on the mechanical properties of the rachis fiber direction: (a) the specific energy absorption distribution law of rachis with and without medulla; the stress–strain curve of S1 rachis: (b) with medulla (c) without medulla
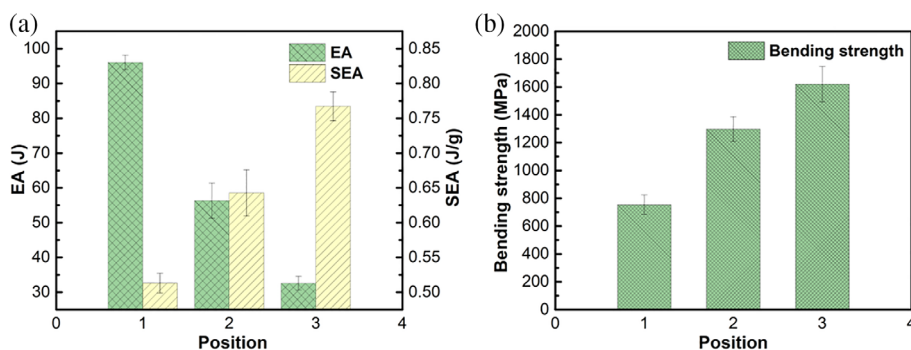
FIGURE 6 The mechanical properties of the fiber direction of the rachis in different areas: (a) the total energy absorption and specific energy absorption of the three consecutive sections of the sample (b) bending strength

F1 sample's energy absorption effect is ideal. Figure 6b shows that the bending strength of the three specimens has increased significantly. Moreover, compared with the round tube, the square tube under the same conditions has greater bending strength and is not easy to deform, and the test results are in line with expectations.

3.3 | Structural analysis test

3.3.1 | The cross section of sample

The rachis is mainly composed of fibrous outer cortex and foamy inner medulla. The cross-sections of the eight rachis specimens of the primary

flight feathers were observed by the 3D microscope system with a super wide depth of field. As can be seen from Figure 7, the proximal shaft cross-sectional shape of the N1 is almost round, and there is a deep groove on the ventral side. However, the shape changes along the fiber direction, the cross-sectional shape gradually evolves into a square shape, and the groove gradually becomes shallower. Second, the cortex on the two sides close to the pinna is very thin, while the cortex on the other two sides is thicker, and the cortex on the dorsal side of the rachis has a ridge (similar to a reinforced ridge), which adds longitudinal reinforcement. The cortex is composed of longitudinal fibers. This fiber arrangement is usually used in the design of synthetic composite materials to inhibit the separation of axial fibers by preventing axial splitting during bending. There are no support plates in the rachis and most of them are
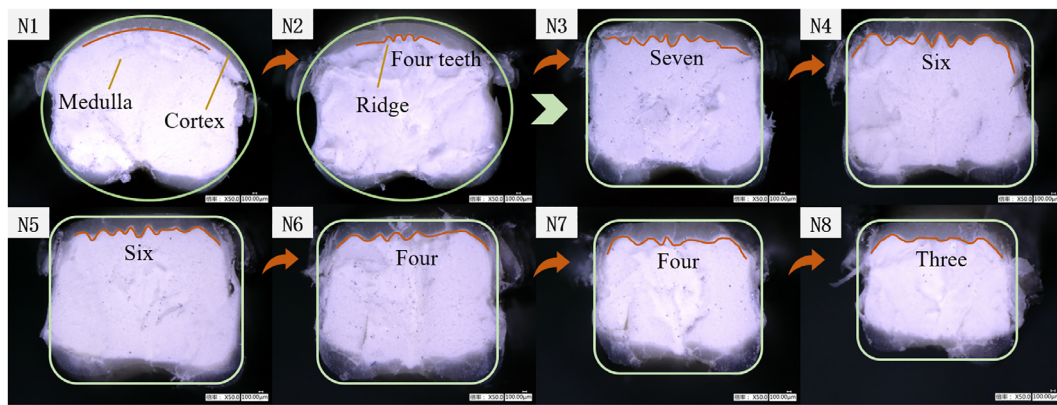
FIGURE 7 The change of cross-section along rachis fiber direction

foam-filled. Foamy medulla is considered closed-cell and absorbs a lot of energy, making the strength of the entire rachis higher. Moreover, the foam medulla can delay local buckling, adapt to and adjust the deformation of the cortex, and absorb a large amount of energy through cell deformation, and wall buckling and rupture (McKittrick & Yang, 2013). Combined with the change law of the cross-section of the rachis, its cross-section gradually evolves from an approximate circle to a square (from N1 to N8). Under the same cross-sectional area and thickness, the square tube has higher stiffness per unit area than the round tube (Wang & Meyers, 2017), so the closer to the distal shaft, the smaller deformable of the rachis specimen.

3.3.2 | Micro-CT results

Based on the above test results, the mechanical properties of N3 specimen are better. A section at this position of the rachis is selected and observed with Xradia 610 Versa 3D X-ray microscope. Figure 8a is the 3D Viewer software of ZEISS, which can observe the reconstructed 2D slice. Each quadrant represents a different orthogonal virtual slice. The colored lines correspond to the same border color slice. By moving the color line, you can see the virtual slice change of the corresponding color wire frame. The three pictures in Figure 8b are virtual slices taken at different positions in the same direction with a voxel resolution of 2.25 μm. The microstructure of the rachis can be clearly seen. There is a groove on one side of the rachis and the other side has structural ridges to strengthen the internal structure; the dense foamy medulla inside increases its energy absorption capacity. At the same time, from the proximal shaft to the distal shaft, the number of teeth of the structural ridge shows a decreasing trend. In addition, based on the observation results, a 3D model of the 7-tooth specimen was reconstructed.

### 3.4 | The analysis of mechanical properties of 3D reconstructed model

The observed cross-section images by micro-CT (Figure 8) were imported into the Solidworks2016 to establish the 3D reconstructed model

of rachis, as shown in Figure 9a. Its height is 80 mm. The 3D model has two parts, including cortex (yellow) and medulla (gray), as shown in Figure 9b. After assembly, it was imported into ANSYS Workbench 19.2. The meshing diagram was shown in Figure 9c. A hexahedral method is used to divide the mesh. The minimum element size is 3 μm. The number of elements in the rachis model is 413,700 and the number of nodes is 1,900,405. And the model was compressed along the Z axis at a constant speed of 2 mm/min. As shown in Figure 9d, the total compress displacement was 5.61 mm.

Although the cortex and medulla of the rachis are almost entirely composed of β-keratin, their density is quite different. The density of the medulla is $0.037 \sim 0.08$ g/cm^3, and the density of the cortex is $0.66 \sim 0.81$ g/cm^3(Wang & Sullivan, 2017). The cortex is more than 100 times harder than foamy medulla. Due to this great elasticity, the geometry of the cortex dictates the bending stiffness of the rachis. Feathers are composed of fibers that are oriented in such a way to maximize resistance to bending and twisting, which undoubtedly increases the complexity of the hierarchy. The keratin fibers in the feathers are arranged in different directions to improve their own stability. Integrating the preliminary biological experiments, the finite element model parameter settings are shown in Table 4.

In order to analyze the compressive performance of the model, all the degrees of freedom at the bottom of the model were restricted, and pressure was applied to the upper end of the model to a size of 104 N. The equivalent stress diagram and equivalent strain diagram of the model were obtained (Figure 10).

Figure 10a is the equivalent stress diagram of the model. It can be seen that under the action of axial pressure, the equivalent stress of the medulla model is very small, and the maximum stress value is concentrated at the junction of the two semicircles and the sawtooth of the cortex model. Because the load is basically carried by these two places, the stress on the surrounding area is relatively small, and the stress at the semicircular joint and the sawtooth is relatively large. It shows that these two places play a certain role in supporting and relieving stress. It also shows that these two areas are the load bearing region, and the mechanical properties of the model is related to the cross-sectional structure. The maximum
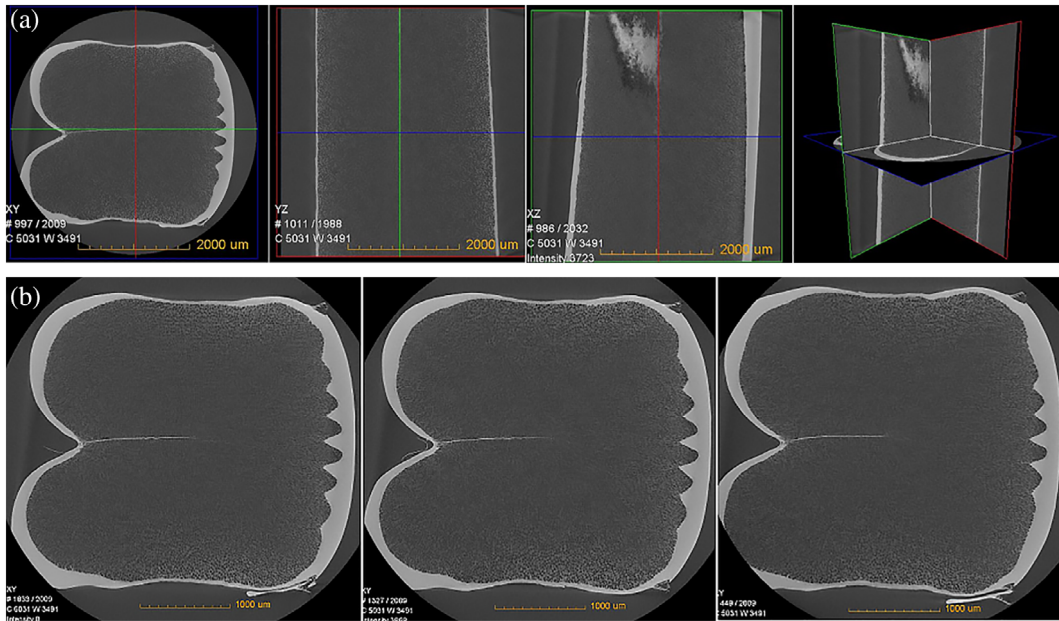
FIGURE 8   (a) The scanning result of rachis and (b) the virtual slices of different positions in the same direction with the 2.25 μm voxel resolution
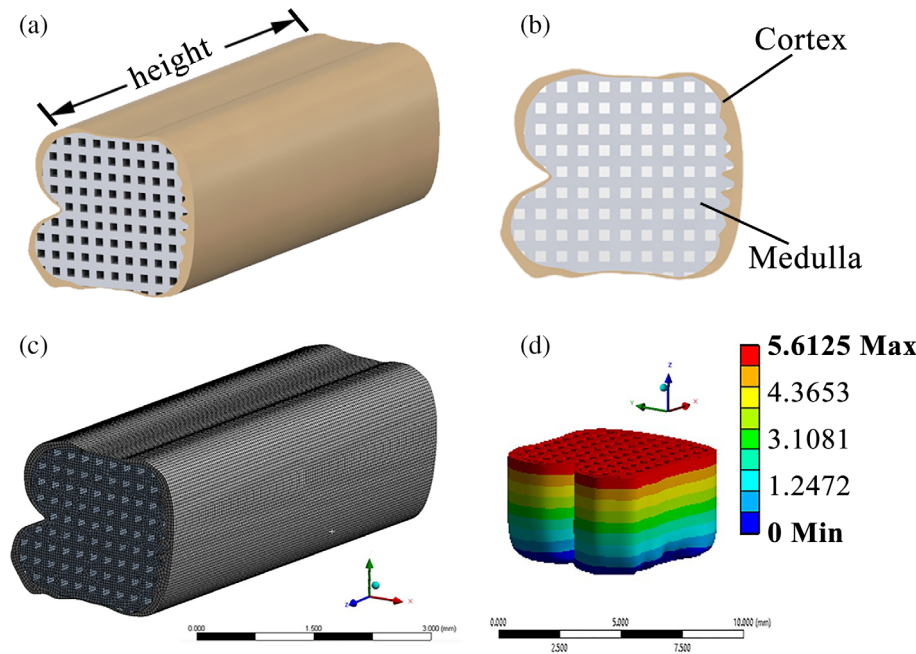

FIGURE 9   (a) 3D reconstructed model of rachis. Its height is 80 mm; (b) cortex and medulla; (c) meshing diagram of the 3D model; (d) the overall deformation of the model

TABLE 4   The parameters of the 3D finite element model

	Value (cortex)	Value (medulla)
Density	0.70 g/cm^3	0.06 g/cm^3
Elastic modulus	500 GPa	4.50 GPa
Poisson ratio	0.3	
Friction factor	0.3	
Compression quality	1000 kg	
Squeezing velocity	2 mm/min	

stress of the model is 643 GPa and the minimum stress is 723.82 MPa. Figure 10b is the equivalent strain diagram of the model. The analysis found that when the model is under pressure, the strain in the early stage increases uniformly, and the strain at the semicircular joint in the later stage increases significantly, which is quite different from other areas. Therefore, this structural feature is suitable for the design of energy absorption, and the structural parameters of these two places were extracted, which can improve the energy absorption characteristics.
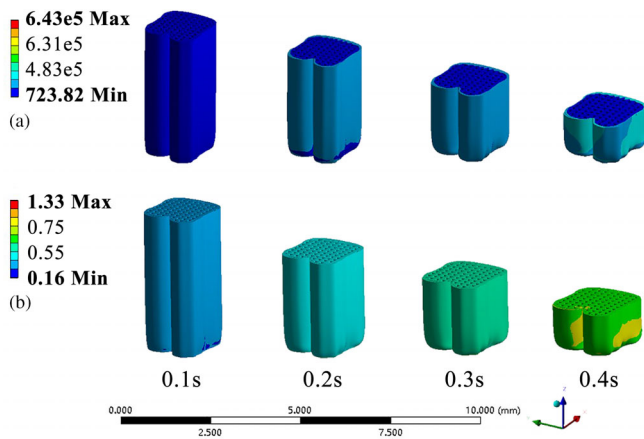
FIGURE 10 (a) The equivalent stress and (b) the equivalent elastic strain cloud diagram of 3D finite element model

4 | CONCLUSION

In this study, the compressive capacity, bending performance and internal structure of the bean goose's primary feather shaft in different areas along the fiber direction were studied. The 3D reconstructed model of the rachis specimen with best performance was established. And the axial compression statics of 3D model was analyzed by Ansys Workbench 19.2. Therefore, the conclusions are as follows:

1. From N1 to N8, the elastic modulus and bending strength of the rachis specimens gradually increase; the compressive performance first increases and then decreases. At the same time, the compressive performance of the rachis without medulla shows the same trend. However, compared with the rachis with medulla, the compression resistance of the specimens in each area of the rachis without medulla is greatly reduced, which proves that the medulla plays a vital role in the compression performance of the rachis.

2. The mechanical properties of the rachis are related to the cross-sectional structure. The simulation results of the rachis of the N3 sample show that the maximum stress is concentrated at the junction of the two semicircles and the sawtooth of the cortex model, and these two places play a certain role in supporting the entire model and alleviating stress.

3. From the proximal shaft to the distal shaft, the cross-sectional shape gradually evolves from round to square. There are structural ridges inside the dorsal side of the rachis cortex, and the number of teeth on the structural ridges first increases and then decreases, up to seven.

4. The elastic modulus and bending strength of the rachis in fiber direction increase gradually; the compressive performance increases first and then decreases (the rachis with medulla and the rachis without medulla).

CONFLICT OF INTEREST

The authors report no declarations of interest.

DATA AVAILABILITY STATEMENT

The data that support the findings of this study are available from the corresponding author, [C. Liu], upon reasonable request.

ORCID

Chao Liu https://orcid.org/0000-0003-3894-5061
Xiujuan Li https://orcid.org/0000-0002-4972-3088
Yansong Liu https://orcid.org/0000-0001-9667-4023
Yingchun Qi https://orcid.org/0000-0003-4117-2522
Jiyu Sun https://orcid.org/0000-0002-7056-0981
Meng Zou https://orcid.org/0000-0003-0498-4791

REFERENCES

Astbury, W. T., & Marwick, T. C. (1932). X-ray interpretation of the molecular structure of feather keratin. *Nature*, *130*, 309–310.

Chen, Q., Pugno, N. M., & Li, Z. (2020). The rotation toughening mechanism of barb–barbule joint in the barb delamination of feathers. *Acta Mechanica*, *231*, 1173–1186.

Eder, H., & Fiedler, W. (2017). Bionik of flight feathers. *Biologie in Unserer Zeit*, *47*, 54–59.

Laurent, C., Ahmed, S., & Boardman, R. (2019). Imaging techniques for observing laminar geometry in the feather shaft cortex. *Journal of Microscopy*, *277*, 154–159.

Laurent, C. M., Dyke, J. M., & Cook, R. B. (2020). Spectroscopy on the wing: Investigating possible differences in protein secondary structures in feather shafts of birds using Raman spectroscopy. *Journal of Structural Biology*, *211*(1), 1–8.

McCoy, D. E., Feo, T., & Harvey, T. A. (2018). Structural absorption by barbule microstructures of super black bird of paradise feathers. *Nature Communications*, *9*(1), 1–8.

McKittrick, J., & Yang, W. (2013). Separating the influence of the cortex and foam on the mechanical properties of porcupine quills. *Acta Biomaterialia*, *9*, 9065–9074.

Oorschot, B. K., Choroszucha, R., & Tobalske, B. (2020). Passive aeroelastic deflection of avian primary feathers. *Bioinspiration & Biomimetics*, *15*, 056008.

Saey, T. H., & Dietmar, W. H. (2006). A comparison of micro CT with other techniques used in the characterization of scaffolds. *Biomaterials*, *27*(8), 1362–1376.

Schelestow, K., Troncoso, O. P., & Torres, F. G. (2017). Failure of flight feathers under uniaxial compression. *Materials Science and Engineering: C*, *78*, 923–931.

Sullivan, T. N., Meyers, M. A., & Arzt, E. (2019). Scaling of bird wings and feathers for efficient flight. *Science Advances*, *5*, eaat4269.

Sullivan, T. N., Wang, B., & Espinosa, H. D. (2017). Extreme lightweight structures: Avian feathers and bones. *Materials Today*, *20*, 377–391.

Sullivan, T. N., Zhang, Y., & Zavattieri, P. D. (2018). Hydration-induced shape and strength recovery of the feather. *Advanced Functional Materials*, *28*(30), 1–9.

Wang, B., & Meyers, M. A. (2016). Seagull feather shaft: Correlation between structure and mechanical response. *Acta Biomaterialia*, *48*, 270–288.

Wang, B., & Meyers, M. A. (2017). Light like a feather: A fibrous natural composite with a shape changing from round to square. *Advanced Science*, 4(3), 1–10.

Wang, B., & Sullivan, T. N. (2017). A review of terrestrial, aerial and aquatic keratins: The structure and mechanical properties of pangolin scales, feather shafts and baleen plates. *Journal of the Mechanical Behavior of Biomedical Materials*, 76, 4–20.

Wang, B., Yang, W., & McKittrick, J. (2016). Keratin: Structure, mechanical properties, occurrence in biological organisms, and efforts at bio-inspiration. *Progress in Materials Science*, 76, 229–318.

Xing, L., Cockx, P., & McKellar, R. C. (2019). Ornamental feathers in cretaceous Burmese amber: Resolving the enigma of rachis-dominated feather structure. *Journal of Palaeogeography*, 7(13), 1–18.

Zhao, J., Zhang, J., & Zhao, Y. (2020). Data of feather recovering performance of birds and micro structure of pigeons' feathers. *Data in Brief*, 29, 105100.

Zou, M., Xu, L., & Zhou, J. (2020). Microstructure and compression resistance of bean goose (*Anser fabalis*) feather shaft. *Microscopy Research and Technique*, 83(3278), 156–164.

Zou, M., Zhou, J., & Xu, L. (2019). An engineering perspective on the microstructure and compression properties of the seagull Larus argentatus feather rachis. *Micron*, 126, 102735.